water

MDPI

*Article*

# Synthesis of Magnesium Modified Biochar for Removing Copper, Lead and Cadmium in Single and Binary Systems from Aqueous Solutions: Adsorption Mechanism

**Yu Deng [1,2,3], Xiaodong Li [1,2], Fuquan Ni [3], Qiao Liu [3], Yunpeng Yang [3], Min Wang [3], Tianqi Ao [1,2,*] and Wenqing Chen [4,*]**

[1] State Key Laboratory of Hydraulics and Mountain River Engineering, Sichuan University, Chengdu 610065, China; yudeng21@sicau.edu.cn (Y.D.); xiaodongli@scu.edu.cn (X.L.)
[2] College of Water Resources and Hydropower, Sichuan University, Chengdu 610065, China
[3] College of Water Conservancy and Hydropower Engineering, Sichuan Agricultural University, Ya'an 625014, China; nfq1965@163.com (F.N.); liuqiao20120117@163.com (Q.L.); yangyunpeng0625@163.com (Y.Y.); wangmin9969@163.com (M.W.)
[4] College of Architecture and Environment, Sichuan University, Chengdu 610065, China
* Correspondence: aotianqi@scu.edu.cn (T.A.); chenwenqing@scu.edu.cn (W.C.)

**Abstract:** Biochar modification can enhance the properties associated with porosity and functional groups and has been identified as an effective way to improve adsorption capacity. Modified corncob biochars pretreated by different contents of $MgCl_2$ are obtained through slow pyrolysis; then, this work explores the adsorption abilities towards heavy metals. After modification, biochars mainly impregnate carbon surface with $Mg(OH)_2$ and MgO particles. The best mass ratio of magnesium (Mg)/feedback is 15% for modified biochar, and 15%Mg-BC has much higher (2.36–9.34 times) metal sorption capacity than pristine biochar. Batch adsorption experiments show that copper (Cu(II)) and lead (Pb(II)) on adsorbents follow a pseudo-second-order model and cadmium (Cd(II)) follows an intraparticle diffusion model. The adsorption isotherm of Cu(II) fits well with the Langmuir model, and Pb(II) and Cd(II) fit with the Freundlich model. In the binary system, modified biochar still effectively removes metals, but the sorption capacity of metals decreases rapidly because of competitive sorption. The main adsorption mechanisms of metals include surface precipitation, cation π-banding, complexation, and ion exchange. The results show that Mg-modified biochar may be an environmentally friendly material for reducing the water pollution of heavy metals.

**Keywords:** Mg-modified biochar; adsorption; heavy metals; binary system; wastewater



**Citation:** Deng, Y.; Li, X.; Ni, F.; Liu, Q.; Yang, Y.; Wang, M.; Ao, T.; Chen, W. Synthesis of Magnesium Modified Biochar for Removing Copper, Lead and Cadmium in Single and Binary Systems from Aqueous Solutions: Adsorption Mechanism. *Water* **2021**, *13*, 599. https://doi.org/10.3390/w13050599

Academic Editor: Antonio Zuorro

Received: 15 January 2021
Accepted: 22 February 2021
Published: 25 February 2021



## 1. Introduction

According to the National Soil Pollution Survey Bulletin of China, soil heavy metal pollution (especially Cu, Cd, and Pb) is getting worse in many cultivated fields and mining areas [1]. Studies have shown that industrial wastewater and mining wastewater are important sources of heavy metal pollution in soil, as shown in references [2,3]. Heavy metals have the features of toxicity and nonbiodegradation, and they may not only cause various ecological and environmental problems [4], but also pose a threat to human health via food since they can accumulate in animals and vegetations [5,6]. Therefore, an effective technology for removing heavy metals from sewage is urgently required.

Several methods (e.g., adsorption, chemical precipitation methods, advanced oxidation, electrochemical methods, and bioaccumulation) have been successfully applied to treat heavy metals [7–9], among which adsorption is an important clean technology in the treatment process. Furthermore, adsorbents such as activated carbon [10], carbon nanomaterials [11], graphene materials [12], and biosorbents [13] have been adopted to reduce metals, but these materials have high costs and complicated operations [11]. Biochar as a new efficient and inexpensive material has been widely applied in environmental

pollution remediation. It is prepared by pyrolysis and carbonization of agricultural wastes under limited oxygen or anaerobic conditions [14], and thus has the advantages of rich functional groups, porous structure, high exchangeable cation, and large specific surface area [15]. Due to the abundant feedstock and simple preparation method, biochar has been regarded as an effective adsorbent with acceptable low cost and is widely applied to remove heavy metals as an adsorbent [16,17].

Nevertheless, the adsorption capacity of pristine biochar on pollutants is limited by its texture, especially when wastewater contains high concentration of contaminants [18,19]. This means that the properties of biochar need to be improved to increase its sorption capacity [18]. The modifying method of coating metal oxides (e.g., MgO, $Fe_xO_y$, ZnO, and $MnO_x$) on the feedstock or the prepared biochar is one of the commonly used methods [18–22]. Compared with pristine biochars, the metal-modified biochars can significantly enhance the properties of functional groups (–COOH, –OH, and –C=O), surface specific areas, pore structures, and cation exchange capacity (CEC) [14,23], and thus can provide more adsorption sites for heavy metals [23]. However, the different adsorption processes and mechanisms of metal-modified biochars are different. Li et al., found that the sorption kinetics of Cd(II) on BC-$MnO_x$ follows a pseudo-second-order model, and the main mechanisms involve cation exchange and cation-π bonding [24]. Ifthikar et al. reported that magnetic biochar adsorbed Pb(II) which is well-described by a pseudo-second-order model; the adsorption mechanisms involve electrostatic attraction, ion exchange, complexation and precipitates [25]. Moreover, Nnadozie and Ajibade observed that Fe leached percentages of $Fe_3O_4$@BC/APTES are 8.55% and 4.42%, respectively, after 1 h in acidic and neutral conditions [22], indicating that the metal oxides coated on biochars may dissolve and cause secondary pollution, so it is very important to select environmentally friendly metal-modified materials. Recently, Mg-modified biochars have attracted wide attention for their low toxicity and high adsorption capacity [20,21], and they have been found to significantly enhance the properties and the adsorption capacity of Cr(VI), increasing from 20.79 to 54.64 mg/g [20]. Mg-modified biochars are mainly coated by particles of MgO and $Mg(OH)_2$, which are different products under different pyrolysis conditions [26]. Magnesium chloride ($MgCl_2$) is one of the reagents to decompose the magnesium oxide particles. However, the amount of $MgCl_2$ loaded on the biomass is unclear, which makes it difficult to control the final Mg content of biochar.

Here, this study aims to (1) investigate the physicochemical properties of different contents of magnesium-modified biochars, (2) study the impact of Mg contents, pH, and dosage on adsorption capacity of heavy metals, (3) explain the mechanisms of heavy metals by batch experiments of sorption kinetics and isotherms, (4) explore the influences of metal sorption onto modified biochar under coexisting metal systems, and (5) discuss the adsorption mechanisms of 15%Mg-BC through analytical testing technology.

## 2. Methods and Materials

### *2.1. Materials*

Corncob was obtained from local farmland in Ya'an City, Sichuan Provence, China (29°58′50″ N, 103°1′23″ S). Dried biomass was milled into fine particles of 1 mm before use. All chemicals, copper(II) chloride dehydrate (≥99.0%), magnesium chloride hexahydrate (≥98.0%), lead nitrate (≥98.0%), cadmium chloride (≥99.0%), and sodium hydroxide (≥98.0%), all of analytical grade, were purchased from Chengdu Chron Chemicals Co., Ltd. Deionized (DI) water (18.25 MΩ) (UPH-IV-10T, Ulupure) was used in the experiments.

### *2.2. Biochar Preparation*

In order to prepare modified biochar, 5.0 g of biomass was soaked in 50.0 mL of $MgCl_2 \cdot 6H_2O$ solution and controlled the Mg/biomass mass ratios of 5%, 10%, 15%, and 20%, respectively. The resulting dispersion underwent ultrasonic irradiation for 2 h at room temperature and was then dried at 80 °C. After that, the prepared Mg biomass composites were pyrolyzed in a muffle furnace under $N_2$ atmosphere. The temperature was raised

from room temperature to 450 °C at a heating rate of 10 °C/min, and the peak temperature was maintained for 1 h. The obtained biochar sample was washed by deionized water several times to clean ash. Subsequently, the washed sample was dried in an oven at 80 °C and crushed into particles through 40 mesh (0.45 mm) and denoted as xMg-BC (x = 5%, 10%, 15%, and 20%). The untreated biomass was prepared under the same conditions as the controls and is noted as BC.

### 2.3. Characterization

The biochars before and after adsorbing heavy metals were characterized by the following techniques. The element compositions of C, O, H and N were analyzed by elemental analyzer (Vario Macro Cube, Germany) and the metals of biochars were examined by inductively coupled plasma optical emission spectroscopy (ICP-OES) (PerkinElmer Optima 8000, Waltham, USA). The surface area and pore structure properties of adsorbents were performed by the Brunauer–Emmett–Teller (BET) multilayer adsorption isotherm (Quadrasorb 2MP, USA). The surface functional groups of BC and xMg-BC were characterized by Fourier transform infrared spectroscopy (FTIR) (Nicolet iS20, Thermo Scientific, Waltham, USA). The surface morphological structures were detected by scanning electron microscopy (SEM) (ZEISS Evo18 500, Jena, Germany). The crystal structures of metal minerals were investigated through an X-ray diffractometer (XRD) (PANalytical X' Pert Powder, Alemlo, Netherlands). The element compositions and combination states of adsorbents before and after metal adsorption were measured via X-ray photoelectron spectroscopy (XPS) (Esclab 250Xi, Thermo Scientific, Waltham, USA).

The $pH_{PZC}$ of xMg-BC and BC were examined by the method described in the previous study [21]. In brief, 50 mL NaCl solution (0.1 M) was added into a centrifuge tube (100 mL) and 0.1 M NaOH or HCl was used to adjust the initial pH ($pH_i$) of the solution to within 2–12. Then, 0.01 g of biochar was put into the solution. After, the biochar was incubated 48 h, and the final pH of suspension solution was measured and noted as $pH_f$. The $pH_{PZC}$ of biochars was computed by the equation ($\Delta pH = pH_f - pH_i = 0$).

### 2.4. Influence of Mg Content, Dosage, and Initial pH

To assess effect of the Mg content on heavy metal adsorption, 0.01g of the adsorbent was added into 100 mL centrifuge tube containing 50 mL of each heavy metal solution. The influence of dosage on adsorption capacity of materials (15%Mg-BC) was investigated at weight values (0.001, 0.005, 0.01, 0.05, and 0.1 g) in 50.0 mL of solution. In order to study the impact of initial pH on the adsorption performance towards metal ions, the batch experiments were performed with different pH values (2.0, 3.0, 4.0, 5.0, and 6.0) using 0.1 M NaOH or HCl. When pH > 6, parts of metal ions were not stable and formed precipitation [20]. Cu(II), Cd(II), and Pb(II) concentrations in the system were 50.0, 50.0, and 100 mg/L, respectively. The mixture was incubated at 180 rpm and 25 °C for 24 h and then filtered through an 0.45 μm membrane, and ICP-OES was used to detect the concentration of filtrate.

### 2.5. Batch Experiments

Sorption kinetics of metal ions onto the adsorbents were explored by adding 0.01 g of 15%Mg-BC into a 100 mL centrifuge tube containing 50.0 mL of 50.0 mg/L Cd(II), 50.0 mg/L Cu(II), and 100.0 mg/L Pb(II), respectively. The initial pHs of the solutions were adjusted to 5.0, which has been demonstrated to be the optimal by the above experiments. Subsequently, the suspensions were shaken at 180 rpm and 25 °C for equilibration sorption, and samples were collected at 0.5, 1.0, 2.0, 4.0, 6.0, 8.0, 10.0, 16.0, and 24.0 h.

Sorption isotherm experiments of heavy metals were conducted by adding 50.0 mL of Pb(II) (50.0 to 150.0 mg/L), Cu(II), and Cd(II) (10.0 to 100.0 mg/L) into a 100 mL centrifuge tube containing 0.01 g of modified BC; then, the mixture was incubated at 180 rpm and 25 °C for 24 h. After the studied system reached the equilibrium state, the concentrations

of heavy metal ions were detected to determine variations in the solutions so as to establish a suitable isotherm model.

### 2.6. Binary System

The binary system of metals was conducted in order to investigate the influences on adsorption under metal ions coexistence. Firstly, the system concentrations of Cd(II) and Cu(II) were controlled at 50.0 mg/L, and that of Pb(II) was controlled at 100 mg/L. Then, the mixed coexisting metal concentration was regulated from 0.0 to 50.0 mg/L for Cd(II) and Cu(II), and from 0.0 to 100.0 mg/L for Pb(II). Finally, 50.0 mL of mixed solution at a pH value of 5.0 was added into a 100 mL centrifuge tube containing 0.01 g 15%Mg-BC and was shaken for 24 h. The suspensions were filtered through 0.45 μm membrane (PES).

## 3. Results and Discussion

### 3.1. Properties of Biochar

The physicochemical properties of BC and xMg-BC are shown in Table 1. It can be observed that Mg was successfully loaded onto modified biochar (XRD patterns also confirmed this) and that its element compositions and pore structures changed. xMg-BC has a C content of 42.79–59.61%, which is lower than that of BC (77.25%). The contents of H and O in modified biochar increased from 3.027 and 18.75 (BC) to 3.35–4.55% and 26.52–33.51%, respectively, which were enhanced with increasing Mg. Compared with BC, the H/C and O/C obtained in xMg-BC are larger, which indicates that Mg-coated BC contributes to retaining H and O contents and increasing oxygen functional groups, as well as enhancing the hydrophilicity of xMg-BC [26,27], all of which are favorable to heavy metal adsorption.

**Table 1.** Physiochemical properties of biochars.

| Biochar | Element Composition (%) | | | | | H/C | O/C | pHpzc | $S_{BET}$ ($m^2$/g) | $V_{total}$ ($cm^3$/g) |
|---|---|---|---|---|---|---|---|---|---|---|
| | C | H | O | Mg | Ca | | | | | |
| BC | 77.25 | 3.03 | 18.75 | 0.12 | 0.078 | 0.039 | 0.24 | 8.00 | 12.68 | 0.0232 |
| 5%Mg-BC | 59.61 | 3.35 | 26.52 | 10.07 | 0.007 | 0.056 | 0.45 | 9.97 | 52.41 | 0.1331 |
| 10%Mg-BC | 54.32 | 3.79 | 27.83 | 13.62 | 0.009 | 0.070 | 0.51 | 10.02 | 101.96 | 0.1301 |
| 15%Mg-BC | 49.21 | 3.82 | 29.90 | 16.46 | 0.008 | 0.078 | 0.61 | 9.88 | 174.29 | 0.3106 |
| 20%Mg-BC | 42.79 | 4.55 | 33.51 | 18.52 | 0.007 | 0.106 | 0.78 | 9.93 | 77.0 | 0.2712 |

The pHpzc of biochars is affected by the surface functional groups, and the pHpzc of biochar after modification raises to 9.88–10.02, which is higher than 8.0 of BC, indicating that Mg-modified adsorbents contain more alkaline functional groups and can be favorable for heavy metal adsorption.

The pore structure properties of biochar were improved by modification, and the specific surface area for xMg-BC increased from 12.68 (BC) to 52.41–174.29 $m^2$/g. Moreover, higher pore volumes ($V_{total}$) were observed in the Mg-coated biochars than in BC. The increase in the surface area and pore volumes of modified biochars are ascribed to the improvement of the pore structure when the BC is impregnated with magnesium oxide particles, which is further confirmed by the scanning electron photomicrograph.

To study the surface morphological structures of BC and xMg-BC, SEM images are shown in Figure 1. BC has a smooth and shallow groove surface with some undeveloped porous structures, which are related to small surface area. By contrast, the surface morphologies of xMg-BC are characterized by many hive-like structures, indicating that xMg-BC has well-developed pores containing rough surfaces and a great pore volumes. Some columnar crystal appears at 5%Mg-BC, 10%Mg-BC, and 15%Mg-BC, thus can provide more adsorption sites for heavy metals. However, due to the excessive Mg content of 20%Mg-BC, the carbon skeleton structure is destroyed and agglomerates into blocks, which led $S_{BET}$ and $V_{total}$ to be less than 15%Mg-BC. This indicates that the Mg content

should be controlled at a certain level when the biochar is modified. Thus, according to the results of surface morphology and pore structure, 15%Mg-BC can provide more adsorption sites for heavy metal.

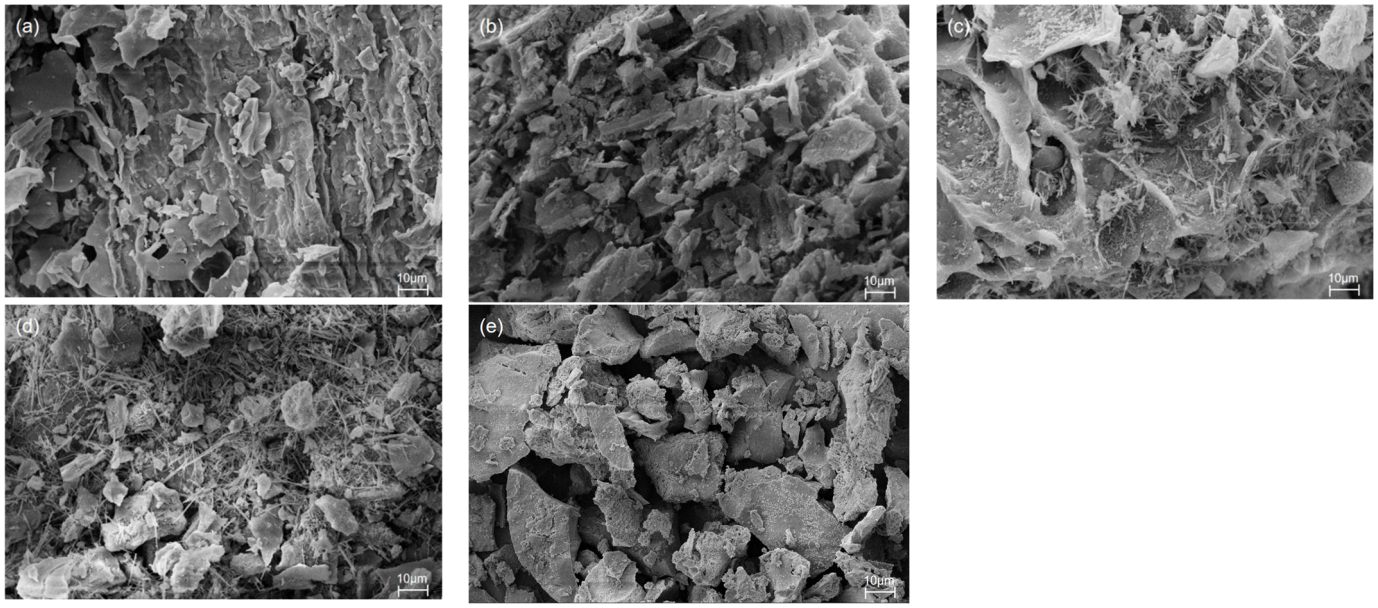


**Figure 1.** Scanning electron microscopy (SEM) images of BC (**a**), 5%Mg-BC (**b**), 10%Mg-BC (**c**), 15%Mg-BC (**d**) and 20%Mg-BC (**e**).

The X-ray diffraction (XRD) patterns displayed well-defined crystal phases and composition structures of biochars, as shown in Figure 2a. In the spectrum of the xMg-BC composite, the peaks have the advantages of high intensities and sharp peak shapes, which are absent in the BC sample. The peaks at 2θ values of 36.9°, 42.9°, and 62.2°, which are related to crystal planes of (111), (200), and (220), respectively, indicate the presence of MgO [28]. Several diffraction peaks of xMg-BC appear at 2θ of 18.56°, 38.05°, 50.89°, 58.72°, 68.31°, 72.14°, and 81.38°. These characteristic diffraction peaks correspond to hexagonal magnesium hydroxide [$Mg(OH)_2$] crystal planes of (001), (101), (012), (110), (013), (021), and (202), respectively [28,29]. As for 5%Mg-BC composites, the sharp peak at 32.13° is assigned to $MgCl_2$ relating to the crystal planes of (011) [22]. Additionally, some weak peaks appear at 2θ values of 29.28° and 33.15°, implying the presence of $CaCO_3$ crystals on BC and xMg-BC [27].

The FTIR transmission spectra of adsorbents show the changes of functional groups, as illustrated in Figure 2b. A new strong absorption peak at 3696 $cm^{-1}$ from the stretching vibration of –OH bond in $Mg(OH)_2$ can be observed for xMg-BC [24], indicating $Mg(OH)_2$ has been loaded on biochar. The peak of 3412 $cm^{-1}$ is verified as caused by the –OH stretching vibration of carboxyl or phenolic hydroxyl [30]. The peak at 1618 $cm^{-1}$ is associated with C=O stretching vibrations of carboxylic groups [31]. The peak of 1440 $cm^{-1}$ may be assigned to the C=O stretching vibrations of aromatic structures [32]. The bond at 845 $cm^{-1}$ is attributed to $CO_3^{2-}$ [33]. The bonds of 608 and 419 $cm^{-1}$ are the bonds of Mg–O stretching vibrations [34].

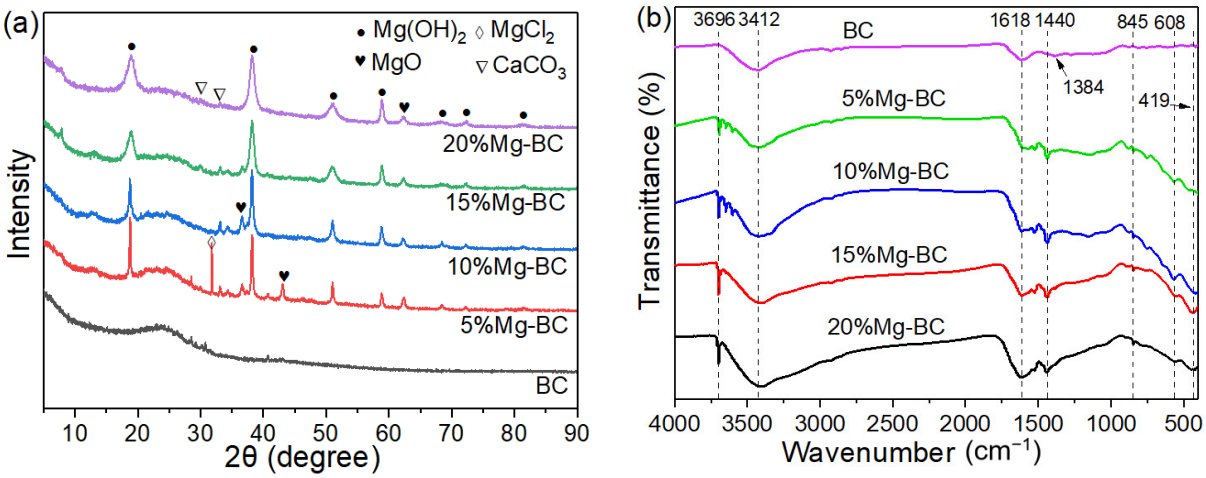


**Figure 2.** X-ray diffraction patterns (**a**) and Fourier transform infrared spectroscopy (FTIR) transmission spectra (**b**) of biochars.

### *3.2. Effects of Mg Content, Dosage, and Initial pH*

The sorption ability of xMg-BC increases in the order of 5%Mg-BC < 10%Mg-BC < 20%Mg-BC < 15%Mg-BC (Figure 3a), indicating the positive effects of heavy metal removal by the Mg-loaded biochars. The metal ions adsorbed by 15%Mg-BC are related to the enhanced biochar pHpzc due to the formation of $Mg(OH)_2$. Therefore, Cu(II), Cd(II), and Pb(II) can be removed through electrostatic interaction to the positively charged surface of biochar when the solution pH is lower than pHpzc [18,21]. For 15%Mg-BC, the sorption capacities of Cu(II), Cd(II), and Pb(II) are 200.33, 164.51, and 448.5mg/g, respectively, about 6.37, 2.36, and 9.34 times higher than BC, suggesting that 15%Mg-BC may be an excellent material for mining wastewater treatment.

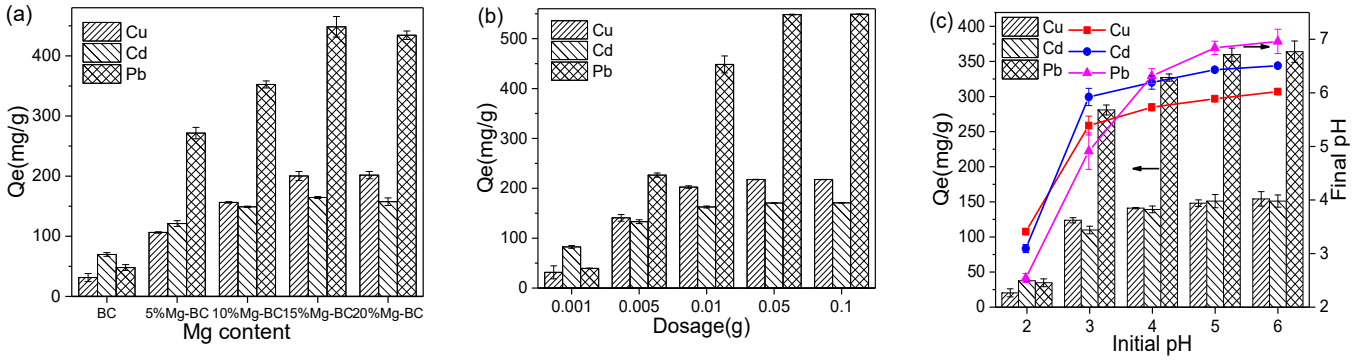


**Figure 3.** The impact of Mg content (**a**), dosage (**b**), and initial pH (**c**) on the sorption of heavy metals by biochars.

The capacity of heavy metal adsorption increases with rising biochar dosage (Figure 3b). For Cu(II), Cd(II), and Pb(II), the sorption capacities increase rapidly from 13.02, 82.47, 32.45 mg/g to 202.3, 162.57, and 448.33 mg/g, respectively, when the modified biochar dosage increases from 0.001 g to 0.01 g. While with the further increase in the dosage, metal ions in the solution are limited, so the capacities of absorbents grow slowly, implying that the appropriate dosage of 15%Mg-BC for metal adsorption is 0.01g.

The solution's initial pH values significantly impact the adsorption of heavy metals by 15%Mg-BC (Figure 3c). The sorption capacities of 15%Mg-BC towards Cu(II), Cd(II), and Pb(II) show a remarkable increase with the increasing initial pH values until they plateau at pH 5.0. When pH is 2.0, the concentration of $H^+$ in the solution is high, and the competitive sorption between $H^+$ and metal ions dominates [30], resulting in low

sorption capacities of 15%Mg-BC. Simultaneously, the abundant $H^+$ leads to protonation of surface functional groups under acidic condition, hindering Cu(II), Cd(II), and Pb(II) sorptions on biochar by electrostatic interactions [35]. As the pH increases, the character of oxygen functional groups (e.g., –OH, and –COOH) changes and the surface of 15%Mg-BC is negatively charged, thus the electrostatic attraction is enhanced, thereby improving the affinity between functional groups and metal cations [31]. This suggests that pH-dependent surface charges play important roles in controlling heavy metal adsorption through electrostatic interactions [18]. Meanwhile, the final pH of solution and the sorption capacities significantly increases when the initial solution pH changes from 2.0 to 3.0. The possible reasons for this are that the release of alkali or the hydrolysis of $Mg(OH)_2$ and MgO particles from the Mg-modified biochar, as well as the rise of the solution pH [20], change the surface of biochar and heavy metal species distribution and increase the affinity of Cu(II), Cd(II), and Pb(II) towards biochar [18]. This process decreases the competitive adsorption between $H^+$ and heavy metals, and the sorption capacities of metals are significantly enhanced.

### *3.3. Sorption Kinetics*

Figure 4 shows the impact of reaction time on the adsorption of Cd(II), Cu(II) and Pb(II) by adsorbents at pH 5.0 and 25 °C. The capacities of 15%Mg-BC for adsorbing Cu(II) and Pb(II) first increase rapidly over time, and then tend to slow down until the reaction reaches equilibrium about 24 h. In contrast, the adsorption of Cd(II) by 15%Mg-BC increases slowly with the contact time, and the sorption equilibrium is not achieved until the test is over.

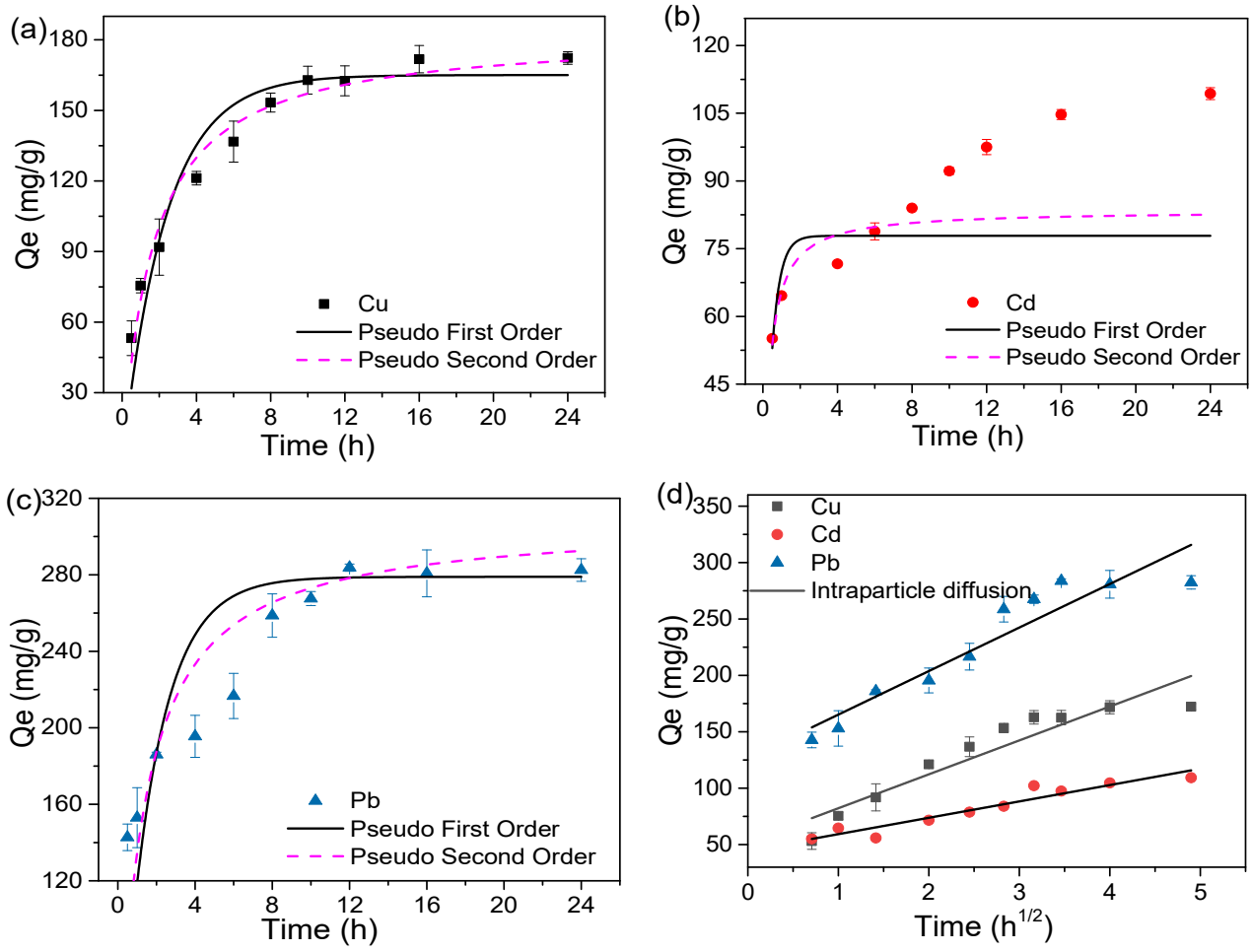


**Figure 4.** Kinetics of 15%Mg-BC for adsorbing Cu(II) (**a**), Cd(II) (**b**), Pb(II) (**c**), and intraparticle diffusion (**d**).

Figure 4 shows the impact of reaction time on the adsorptions of Cd(II), Cu(II), and Pb(II) by adsorbents at pH 5.0 and 25 °C. The capacities of 15%Mg-BC for adsorbing Cu(II) and Pb(II) first increase rapidly over time, and then tend to slow down until the reaction reaches equilibrium after about 24 h. In contrast, the adsorption of Cd(II) by 15%Mg-BC increases slowly with the contact time, and the sorption equilibrium is not achieved until the test is over.

In order to better understand the sorption process, the sorption kinetics of pseudo-first-order, pseudo-second-order and intraparticle diffusion were investigated to fit the experimental data, respectively [36]. The kinetic indexes for metals are presented in Table 2. It can be observed that the sorption processes of Cu(II) and Pb(II) fit well with the pseudo-second-order model because of its high correlation coefficients ($R^2$ = 0.9753 and 0.9499). This indicates that the sorption process is mainly dominated by chemisorption such as cation exchange and precipitation [37]. In addition, the pseudo-second-order model includes intraparticle diffusion, liquid film diffusion, and pore diffusion, which can simulate more accurate sorption processes [36]. For Cd(II), the intraparticle diffusion model fits well with the sorption, and the correlation coefficients are the highest ($R^2$ = 0.9555). Moreover, the intraparticle diffusion model fails to pass through the origin with a high intercept value, which implies that the intraparticle diffusion is not the only controlling factor, and the sorption rate may be affected by the liquid film diffusion and surface adsorption [36].

**Table 2.** Sorption kinetic parameters for Cu(II), Cd(II) and Pb(II) sorption onto 15%Mg-BC.

| Metals | Pseudo-First Order | | | Pseudo-Second Order | | | Intraparticle Diffusion | | |
|---|---|---|---|---|---|---|---|---|---|
| | $\ln(Q_e - Q_t) = \ln Q_e - K_1 \times t$ [a] | | | $t/Q_t = 1/(K_2 \times Q_e^2) + t/Q_e$ [b] | | | $Q_e = K_3 \times t^{0.5} + C$ [c] | | |
| | $K_1$ | $Q_e$ | $R^2$ | $K_2$ | $Q_e$ | $R^2$ | $K_3$ | $C$ | $R^2$ |
| Cu(II) | 0.4278 | 165.03 | 0.8900 | 0.0034 | 182.74 | 0.9753 | 24.6219 | 63.6189 | 0.8552 |
| Cd(II) | 2.2810 | 77.86 | 0.6175 | 0.0434 | 83.49 | 0.7544 | 13.0719 | 47.3670 | 0.9555 |
| Pb(II) | 0.5546 | 278.93 | 0.9121 | 0.0025 | 308.23 | 0.9499 | 43.1468 | 125.9125 | 0.9429 |

Notes: [a] $Q_e$ and $Q_t$ (mg/g) are the adsorption capacity at equilibrium time and time $t$ (h), $K_1$ ($h^{-1}$) is the adsorption rate constant of pseudo-first order; [b] $K_2$ ($h^{-1}$) is the rate constant of pseudo-second order; [c] $K_3$ ($h^{-1}$) is the rate constant of intraparticle diffusion, and $C$ (mg/g) is a constant.

### *3.4. Sorption Isotherms*

The sorption isotherms are used to explain the sorption mechanism of metals by 15%Mg-BC, and the isotherms model can describe the distribution of heavy metals between solution and the adsorbent phase in the sorption process [37]. It is found that the adsorption capacities of modified biochar towards heavy metals increase with the rising initial solution concentration, and then reach the equilibrium (Figure 5). The equilibrium sorption capacities of Cu(II), Cd(II), and Pb(II) in experiment data are 296.85, 180.93, and 527.67 mg/g, respectively.

Some typical models such as the Langmuir and Freundlich models are used to analyze test data [30,38], and the simulation results are shown in Figure 5 and Table 3. It can be seen that the sorption isotherms of Cu(II) fit better with the Langmuir model because the correlation coefficients ($R^2$ = 0.9547) are larger, indicating that it is a monolayer absorption of adsorbate on the homogeneous surface [31,39]. The Freundlich model for Cd(II) and Pb(II) can fit better than Langmuir model with the higher correlation coefficients ($R^2$) of 0.9991 and 0.9974, respectively. The Freundlich model shows that the sorption sites are not evenly distributed and the adsorption occurs on a heterogeneous surface [39]. These results indicate that the sorption processes of copper, lead, and cadmium onto 15%Mg-BC are controlled by different adsorption mechanisms. Furthermore, the parameter of $K_L$ values at 0 to 1 indicates that 15%Mg-BC has a good adsorption effect on metals [40]. Additionally, the values of $1/n$ in Freundlich model are below 1, indicating that the adsorption process is easy to achieve [41].

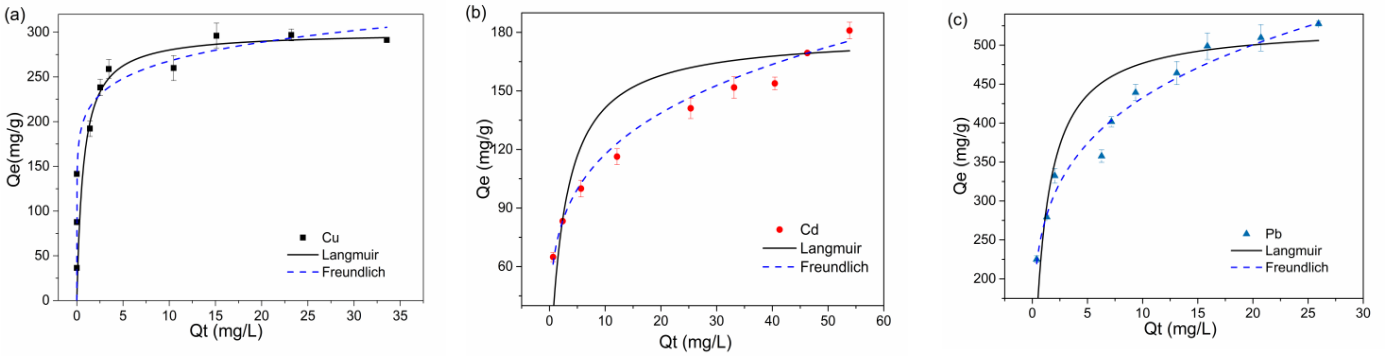


**Figure 5.** Sorption isotherms of Cu(II) (**a**), Cd(II) (**b**), and Pb(II) (**c**) sorption by 15%Mg-BC.

**Table 3.** Sorption isotherms parameters of Cu(II), Cd(II), and Pb(II) sorptions by biochar.

| Metal | Langmuir | | | Freundlich | | |
|---|---|---|---|---|---|---|
| | $Q_e = Q_m \times K_L \times C_e/(K_L \times C_e + 1)$ [a] | | | $Q_e = K_f \times C_e^{1/n}$ [b] | | |
| | $K_L$ | $Q_m$ | $R^2$ | $K_f$ | $n$ | $R^2$ |
| Cu(II) | 0.0078 | 300.20 | 0.9547 | 208.3214 | 9.1769 | 0.9357 |
| Cd(II) | 0.0275 | 178.97 | 0.9788 | 67.9147 | 4.1959 | 0.9991 |
| Pb(II) | 0.0078 | 526.20 | 0.8860 | 266.5197 | 4.7548 | 0.9974 |

Notes: [a] $Q_e$ (mg/g) is the adsorption capacity at equilibrium, $Q_m$ (mg/g) is the maximum adsorption capacity, $K_L$ (L/mg) is the adsorption constant, $Ce$ (mg/L) is the concentration of pollutant at equilibrium, [b] $K_f$ ($(mg^{1-n} \cdot L^n/g)$ is the sorption capacity constant, and $n$ is the sorption density constant of Freundlich.

According to the calculation results of the Langmuir model, the maximum sorption capacities ($Q_m$) of copper, cadmium, and lead on 15%Mg-BC are 300.20, 178.97, and 526.20 mg/g, respectively, which are higher than those of many other materials mentioned in the literature review (Table 4). The reason for the different sorption capacities may be ascribed to the normal potentials of the studied metals [31]. Moreover, it should be pointed out that 15%Mg-BC's affinity with various metals is as follows: Pb(II) > Cu(II) > Cd(II). It can be concluded from the above results that 15%Mg-BC is a high-performance material for controlling heavy metals.

**Table 4.** Adsorption capacity of modified biochars for metal sorption from aqueous solutions.

| Adsorbents | Metal | $Q_{max}$ (mg/g) | Adsorption Conditions | References |
|---|---|---|---|---|
| $KMnO_4$-modified hickory wood biochar | Cu(II) | 153.11 | 2–250 mg/L, pH 6.0, 24 h | [18] |
| | Cd(II) | 34.21 | 2–250 mg/L, pH 6.0, 24 h | |
| | Pb(II) | 28.10 | 2–500 mg/L, pH 6.0, 24 h | |
| Alkali-modified biochar | Pb(II) | 53.6 | 2–250 mg/L, pH 5.0, 24 h, 20 °C | [20] |
| Waste art paper biochar | Pb(II) | 1555 | 200–3000 mg/L, pH 5.0, 24 h, 22 °C | [27] |
| Mg-Fe LDH Kiwi branch biochar | Cd(II) | 30.49 | 0.5–100 mg/L, pH 6.5, 24 h, 30 °C | [34] |
| $CoFe_2O_4$ magnetic biochar | Cd(II) | 17.79 | No data | [35] |
| | Pb(II) | 29.7 | No data | |
| Mg-modified corncob biochar | Cu(II) | 300.20 | 10–100 mg/L, pH 5.0, 24 h, 25 °C | This work |
| | Cd(II) | 178.97 | 10–100 mg/L, pH 5.0, 24 h, 25 °C | |
| | Pb(II) | 526.20 | 50–150 mg/L, pH 5.0, 24 h, 25 °C | |

### *3.5. Binary System*

To explore the impact of the coexistence of metal ions on their mutual sorptions onto 15%Mg-BC, the batch sorption experiments of binary systems were performed by adding Cu(II) (0–50 mg/L), Cd(II) (0–50 mg/L), and Pb(II) (0–100 mg/L) to Cu(II) (50 mg/L), Cd(II) (50 mg/L), and Pb(II) (100 mg/L) fixed at pH 5.0. The results are presented in Figure 6. In the system of coexisting metals, 15%Mg-BC still effectively adsorbs metals

within 24 h, but the sorption capacities of all metals decrease due to competitive sorption. As shown in Figure 6a,b, in the binary systems of Cd-Cu and Cd-Pb, the ability of Cd(II) rapidly decreases from 133.23 to 34.6 and 22.72 mg/g with the increasing concentration of Cu(II) and Pb(II). While the content of Cd(II) changed from 0 to 50 mg/L, the capacities of Cu(II) and Pb(II) slowly decline from 156.4 to 125.02 mg/g, and 292.27to 258.05 mg/g, respectively. This indicates that the affinities of Cu(II) and Pb(II) to 15%Mg-BC were higher than Cd(II) [20]. Meanwhile, on the basis of the kinetics results (Figure 4 and Table 1), the rate-determining step in the adsorption process of Cd(II) was mainly controlled by the intraparticle diffusion, which is different to the adsorption processes of Cu(II) and Pb(II), resulting in a dramatic reduction in the sorption capacity of Cd(II). When Cu(II) and Pb(II) coexist in solutions (Figure 6c), the sorption capacities of which both quickly drop from 156.4 to 80.9 mg/g and 292.27 to 87.25 mg/g with the increasing concentration of coexistent ions. This suggests that Cu(II) and Pb(II) can complete the sorption sites on 15%Mg-BC [18].

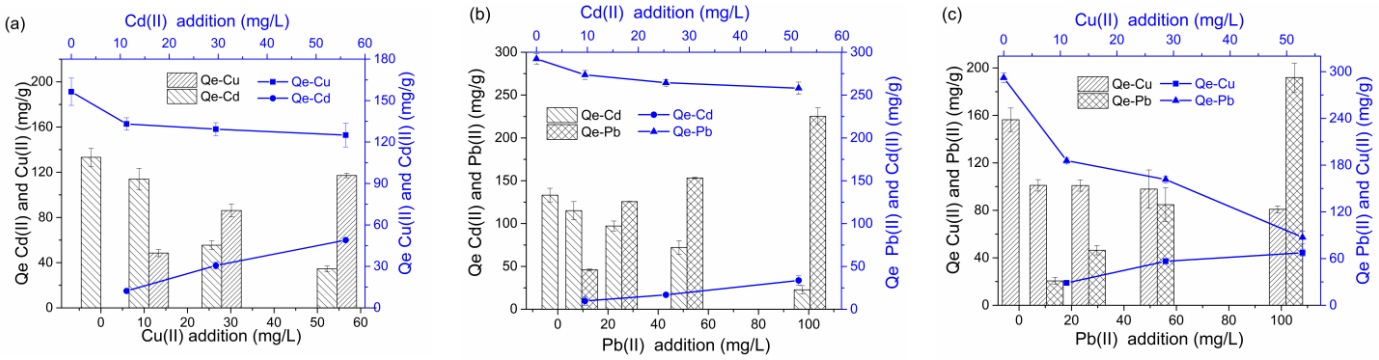


**Figure 6.** The effects of coexisting ions for Cd(II) and Cu(II) (**a**), Cd(II) and Pb(II) (**b**), and Pb(II)and Cu(II) (**c**) adsorption onto 15%Mg-BC.

### *3.6. Adsorption Mechanisms*

The results of adsorption kinetics and isotherms show that heavy metals have individual sorption mechanisms. Thus, in order to better understand the mechanisms, the analytical testing technology, including FTIR, XRD, and XPS, were employed to assess metals after they were adsorbed onto 15%Mg-BC. The results are shown in Figures 7 and 8.

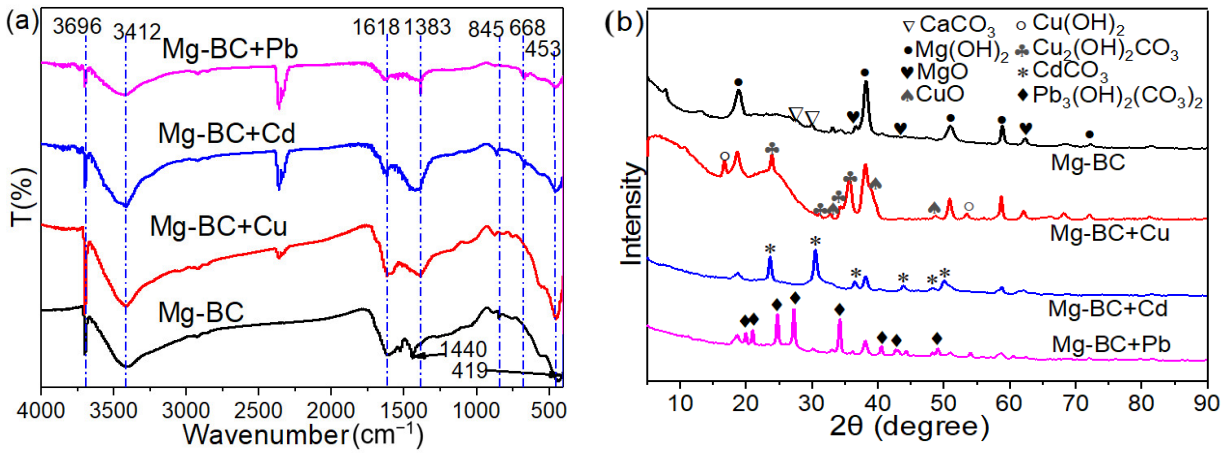


**Figure 7.** FTIR spectra (**a**) and X-ray diffractometry (XRD) patterns (**b**) before and after metal adsorption onto 15%Mg-BC.

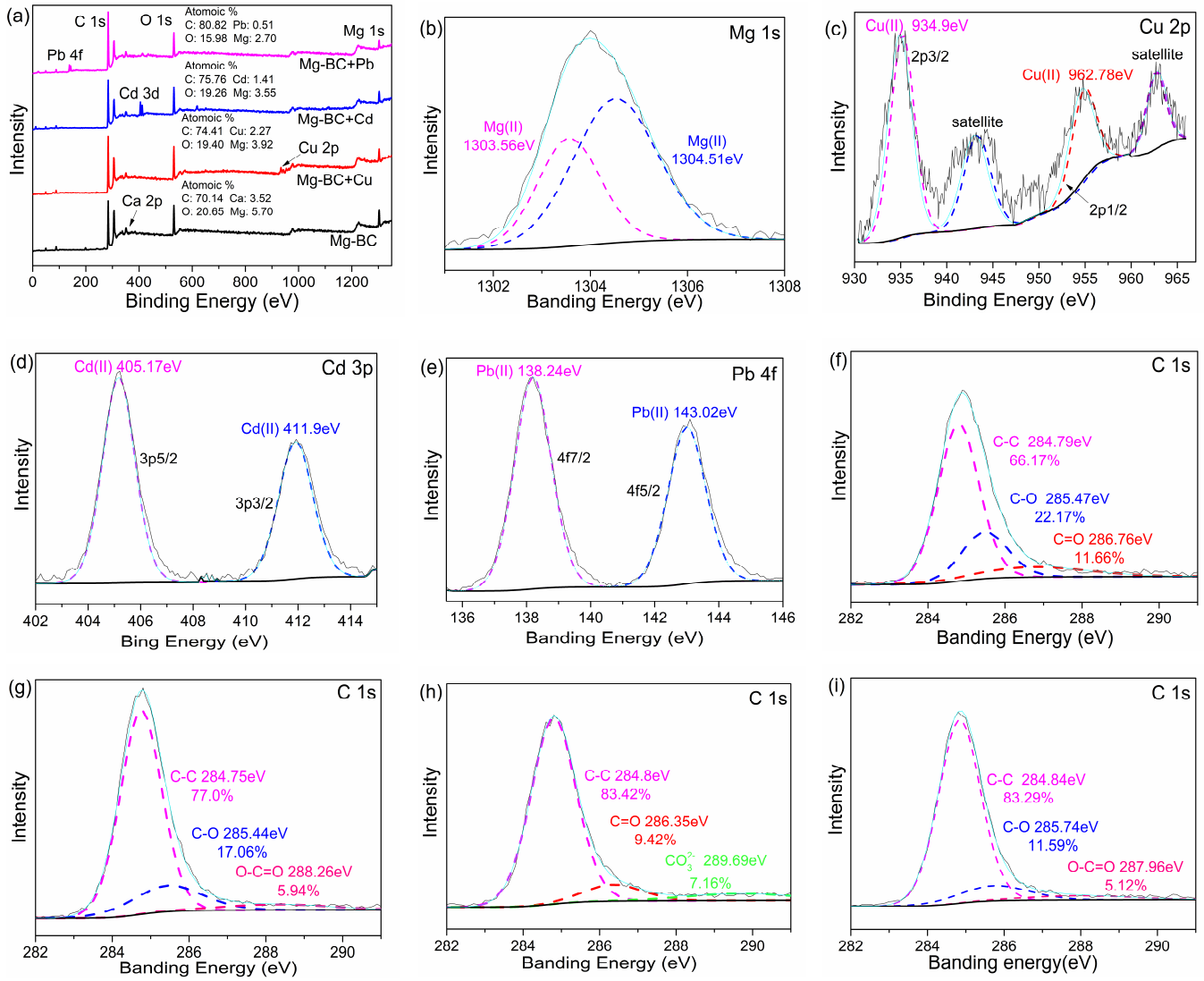


**Figure 8.** X-ray photoelectron spectroscopy (XPS) spectra (full scan) (**a**), 15%Mg-BC (**b**,**f**), and Cu- (**c**,**g**), Cd- (**d**,**h**) and Pb-coated biochars (**e**,**i**).

Figure 7a shows the FTIR spectra regarding the adsorption of heavy metals onto 15%Mg-BC. The peaks of 3696 (–OH), 3412 (–OH), and 1618 $cm^{-1}$ (C=O) weaken after adsorbing Cu(II), Cd(II), and Pb(II), suggesting that precipitation (as confirmed by XRD analyses) and cation π-banding are the adsorption mechanisms [19]. The bond at 1440 $cm^{-1}$ (C–H) shifted to 1383 $cm^{-1}$ after metal loading, indicating that the metals reacted with carboxyl through surface complexation, and metal chelation was formed on the Mg-modified biochar [32]. The peak at 419 $cm^{-1}$ (Mg–O) shifted to 453–456 $cm^{-1}$. These peaks were verified as metal–O bands, indicating that ion exchange is a significant metal sorption mechanism [19]. Moreover, the ion exchange of metal ions was also observed by XPS (Figure 8a).

The crystal analysis by XRD is an effective method to confirm the different types of crystal phases and compositions contained in materials. Here, XRD spectra were used to identify the final products of metals coated onto adsorbents (Figure 7b). After adsorbing the heavy metals, the intensity of the calcite ($CaCO_3$) peak disappeared, and the peaks of $Mg(OH)_2$ weakened rapidly. These results confirm that the heavy metals adsorbed by 15%Mg-BC are mainly impacted by precipitation through the reaction between $CaCO_3$, $Mg(OH)_2$, and metal ions. Moreover, some new peaks appeared on the spectrum of

metal-loaded biochar and they correlated with the crystals of $Cu(OH)_2$, $Cu_2(OH)_2CO_3$, $CdCO_3$, and $Pb_3(OH)_2(CO_3)_2$. These diffraction peaks are consistent with previous studies [19,24,42]. Therefore, the XRD spectra of adsorption products also demonstrate that precipitation is the dominant mechanism of metal sorption; the process of adsorption may be as follows:

$$CaCO_3 \rightarrow Ca^{2+} + CO_3^{2-} \quad (1)$$

$$Mg(OH)_2 \rightarrow Mg^{2+} + 2OH^- \quad (2)$$

$$aM^{2+} + bOH^- + cCO_3^{2-} \rightarrow M_a(OH)_b(CO_3)_c \text{ M refers Cu, Cd, and Pb} \quad (3)$$

XPS is an important analytical technology to identify sorption mechanisms and it can determine the changes inthe main elements, chemical bonds, and functional groups after metal adsorption. As shown in Figure 6a, the atomic percentages of Cu, Cd, and Pb increase while those of Ca and Mg decrease after adsorbing metals onto the modified biochars, indicating that ion exchange is an important mechanism. The XPS analyses of the metal-loaded materials are shown in Figure 8b–e. According to the XPS database of Thermo Scientific, the binding energies of Pb 4f at 138.2 ± 0.1 eV can be assigned to $Pb_3(OH)_2(CO_3)_2$, at 934.8 ± 0.1 eV to $Cu_2(OH)_2CO_3$, and at 405.1 ± 0.1 eV to $CdCO_3$. Consequently, the adsorption mechanisms of modified biochar removing metals were verified as ion exchange and precipitation. For the spectra of C 1s (Figure 8f–i), the peaks were fitted at the banding energies of 284.79, 285.47, and 286.76 eV in 15%Mg-BC, which are assigned to the C-containing functional groups of C–C, C–O and C=O, respectively [18,43]. After Cu(II), Cd(II) and Pb(II) sorption, the corresponding contents of C–C increase from 66.17% to 77.0%, 83.42%, and 83.29%, respectively. The functional groups of C=O are replaced by O–C=O (288.26 and 287.96 eV) on the Cu(II)- and Pb(II)-coated biochars [18,20], and the groups of C–O transform to $CO_3^{2-}$ for Cd(II) adsorption onto modified biochar (289.29 eV) [27]. This indicates that these functional groups may dominate the adsorption mechanism through cation π-banding and surface complexation of metals. The above results show that heavy metal adsorption on 15%Mg-BC is controlled by multiple processes, and the possible adsorption mechanisms are illustrated in Figure 9.

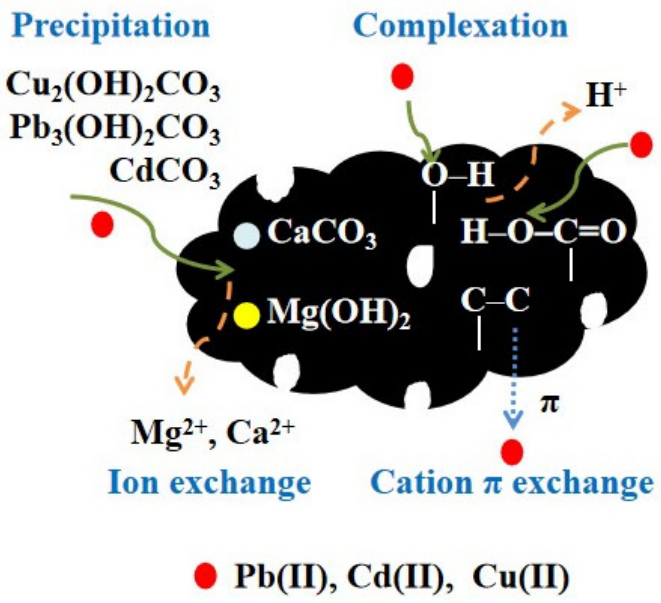


**Figure 9.** Schematic illustration of mechanisms for metal adsorption on 15%Mg-BC.

## 4. Conclusions

In this paper, Mg-modified biochar was prepared by slow pyrolysis with corncob as the raw material. The biochars' properties of oxygen functional groups, porosity, and

specific surface area are improved after modification, and 15%Mg-BC exhibits highly effective sorption capacities of heavy metals in both single systems and binary systems. The experimental results showed that the adsorption isotherm of Cu(II) fits well with the Langmuir model, and the isotherms of Pb(II) and Cd(II) fit well with the Freundluch model. The maximum adsorption capacities of Cu(II), Cd(II), and Pb(II) on 15%Mg-BC calculated from the Langmuir model are 300.20, 178.97, and 526.20 mg/g, respectively. Furthermore, the solution initial pH value is an important factor to affect the sorption capacity of 15%Mg-BC. In this case, the main adsorption mechanisms may be surface precipitation, cation π-banding, complexation, or ion exchange. Thus, 15%Mg-BC can not only easily be prepared, but also has great potential to be used as an adsorbent for controlling water environment pollution.

**Author Contributions:** Y.D., Q.L., Y.Y., and M.W. conducted the experiments; X.L., and F.N. drew the figures and tables; Y.D. fitted the kinetics and isotherm model and was a major contributor in writing of the manuscript. T.A. and W.C. proofread the manuscript and were the major contributors in writing the manuscript. All authors have read and agreed to the published version of the manuscript.

**Funding:** All the funding of the manuscript including reagent, material testing, and proofreading of the paper was from the Major Program of Science and Technology of Sichuan Province (No. 2018SZDZX0028); Sichuan Science and Technology Program (No. 2018RZ0125); Regional Innovation Cooperation Program of Sichuan Province (No. 2020YFQ0013).

**Institutional Review Board Statement:** Ethical review and approval were waived for this study, because this study did not involve humans or animals.

**Informed Consent Statement:** Informed consent was obtained from all subjects involved in the study.

**Data Availability Statement:** The data used to support the findings of this study are available from the corresponding author upon request.

**Acknowledgments:** Our sincere thanks go to Hong Yan at the Faculty of Humanities and Foreign Languages of the Xi'an University of Technology for his edits in improving the quality of this paper.

**Conflicts of Interest:** We declare that we do not have any commercial or associative interests that represent a conflict of interest in connection with the work submitted.

## References

1. CEPA; CLRA. Available online: http://www.gov.cn/foot/site1/20140417/782bcb88840814ba158d01.pdf (accessed on 17 April 2014).
2. Li, Q.; Ji, H.; Qin, F.; Tang, L.; Guo, X.; Feng, J. Sources and the distribution of heavy metals in the particle size of soil polluted by gold mining upstream of Miyun Reservoir, Beijing: Implications for assessing the potential risks. *Environ. Monit. Assess.* **2014**, *186*, 6605–6626. [CrossRef]
3. Wu, J.; Lu, J.; Li, L.; Min, X.; Luo, Y. Pollution, ecological-health risks, and sources of heavy metals in soil of the northeastern Qinghai-Tibet Plateau. *Chemosphere* **2018**, *201*, 234–242. [CrossRef] [PubMed]
4. Hu, B.; Shao, S.; Ni, H.; Fu, Z.; Hu, L.S.; Zhou, Y.; Min, X.X.; She, S.F.; Chen, S.C.; Huang, M.X.; et al. Current status, spatial features, health risks, and potential driving factors of soil heavy metal pollution in China at province level. *Environ. Pollut.* **2020**, *266*, 114961. [CrossRef] [PubMed]
5. Zhang, Y.; Yin, C.; Cao, S.; Cheng, L.; Wu, G.; Guo, J. Heavy metal accumulation and health risk assessment in soil-wheat system under different nitrogen levels. *Sci. Total Environ.* **2018**, *622–623*, 1499–1508. [CrossRef]
6. Wei, J.; Cen, K. Contamination and health risk assessment of heavy metals in cereals, legumes, and their products: A case study based on the dietary structure of the residents of Beijing, China. *J. Clean. Prod.* **2020**, *260*, 121001. [CrossRef]
7. Liang, J.; Zhang, L.; Ye, M.Y.; Guan, Z.J.; Huaung, J.J.; Liu, J.Y.; Li, L.; Huang, S.S.; Sun, S.Y. Evaluation of the dewaterability, heavy metal toxicity and phytotoxicity of sewage sludge in different advanced oxidation processes. *J. Clean. Prod.* **2020**, *265*, 121839. [CrossRef]
8. Ahmed Basha, C.; Bhadrinarayana, N.S.; Anantharaman, N.; Meera Sheriffa Begum, K.M. Heavy metal removal from copper smelting effluent using electrochemical cylindrical flow reactor. *J. Hazard. Mater.* **2008**, *152*, 71–78. [CrossRef] [PubMed]
9. Hao, Z.; Chen, L.H.; Wang, C.L.; Zou, X.Q.; Zheng, F.Q.; Feng, W.H.; Zhang, D.R.; Peng, L. Heavy metal distribution and bioaccumulation ability in marine organisms from coastal regions of Hainan and Zhoushan, China. *Chemosphere* **2019**, *226*, 340–350. [CrossRef]
10. Wu, B.; Cheng, G.; Jiao, K.; Shi, W.; Wang, C.; Xu, H. Mycoextraction by Clitocybe maxima combined with metal immobilization by biochar and activated carbon in an aged soil. *Sci. Total Environ.* **2016**, *562*, 732–739. [CrossRef]

11. Chen, T.; Luo, L.; Deng, S.H.; Shi, G.Z.; Zhang, S.R.; Zhang, Y.Z.; Deng, O.P.; Wang, L.L.; Zhang, J.; Wei, L.Y. Sorption of tetracycline on $H_3PO_4$ modified biochar derived from rice straw and swine manure. *Bioresour. Technol.* **2018**, *267*, 431–437. [CrossRef]
12. Molaei, K.; Bagheri, H.; Asgharinezhad, A.A.; Ebrahimzadeh, H.; Shamsipur, M. $SiO_2$-coated magnetic graphene oxide modified with polypyrrole–polythiophene: A novel and efficient nanocomposite for solid phase extraction of trace amounts of heavy metals. *Talanta* **2017**, *167*, 607–616. [CrossRef] [PubMed]
13. Anastopoulos, I.; Kyzas, G.Z. Progress in batch biosorption of heavy metals onto algae. *J. Mol. Liq.* **2015**, *209*, 77–86. [CrossRef]
14. Wang, L.; Wang, Y.; Ma, F.; Tankpa, V.; Guo, X.; Wang, X. Mechanisms and reutilization of modified biochar used for removal of heavy metals from wastewater: A review. *Sci. Total Environ.* **2019**, *668*, 1298–1309. [CrossRef]
15. Chen, X.; Chen, G.C.; Chen, L.G.; Chen, Y.X.; Lehmann, J.; McBride, M.; Hay, A. Adsorption of copper and zinc by biochars produced from pyrolysis of hardwood and corn straw in aqueous solution. *Bioresour. Technol.* **2011**, *102*, 8877–8884. [CrossRef] [PubMed]
16. Jiang, J.; Xu, R.; Jiang, T.; Li, Z. Immobilization of Cu(II), Pb(II) and Cd(II) by the addition of rice straw derived biochar to a simulated polluted Ultisol. *J. Hazard. Mater.* **2012**, *229–230*, 145–150. [CrossRef]
17. Xu, Z.; Xu, X.; Zhang, Y.; Yu, Y.; Cao, X. Pyrolysis-temperature depended electron donating and mediating mechanisms of biochar for Cr(VI) reduction. *J. Hazard. Mater.* **2020**, *388*, 121794. [CrossRef]
18. Wang, H.; Gao, B.; Wang, S.; Fang, J.; Xue, Y.; Yang, K. Removal of Pb(II), Cu(II), and Cd(II) from aqueous solutions by biochar derived from $KMnO_4$ treated hickory wood. *Bioresour. Technol.* **2015**, *197*, 356–362. [CrossRef]
19. Trakal, L.; Veselská, V.; Šafařík, I.; Vítková, M.; Číhalová, S.; Komárek, M. Lead and cadmium sorption mechanisms on magnetically modified biochars. *Bioresour. Technol.* **2016**, *203*, 318–324. [CrossRef]
20. Xiao, R.; Wang, J.J.; Li, R.; Park, J.; Meng, Y.; Zhou, B.; Pensky, S.; Zhang, Z. Enhanced sorption of hexavalent chromium [Cr(VI)] from aqueous solutions by diluted sulfuric acid-assisted MgO-coated biochar composite. *Chemosphere* **2018**, *208*, 408–416. [CrossRef]
21. Deng, Y.; Li, M.; Zhang, Z.; Jiang, K.L.; Tian, J.J.; Zhang, Y.; Ni, F.Q. Comparative study on characteristics and mechanism of phosphate adsorption on Mg/Al modified biochar. *J. Environ. Chem. Eng.* **2021**, *9*, 105079. [CrossRef]
22. Nnadozie, E.C.; Ajibade, P.A. Adsorption, kinetic and mechanistic studies of Pb(II) and Cr(VI) ions using APTES functionalized magnetic biochar. *Microporous Mesoporous Mater.* **2020**, *309*, 110573. [CrossRef]
23. Ding, Z.; Hu, X.; Wan, Y.; Wang, S.; Gao, B. Removal of lead, copper, cadmium, zinc, and nickel from aqueous solutions by alkali-modified biochar: Batch and column tests. *J. Ind. Eng. Chem.* **2016**, *33*, 239–245. [CrossRef]
24. Li, B.; Yang, L.; Wang, C.Q.; Zhang, Q.P.; Liu, Q.C.; Li, Y.D.; Xiao, R. Adsorption of Cd(II) from aqueous solutions by rape straw biochar derived from different modification processes. *Chemosphere* **2017**, *175*, 332–340. [CrossRef] [PubMed]
25. Ifthikar, J.; Wang, J.; Wang, Q.L.; Wang, T.; Wang, H.B.; Khan, A.; Jawad, A.; Sun, T.T.; Jiao, X.; Chen, Z.Q. Highly Efficient Lead Distribution by Magnetic Sewage Sludge Biochar:Sorption Mechanisms and Bench Applications. *Bioresour. Technol.* **2017**, *238*, 399–406. [CrossRef]
26. Creamer, A.E.; Gao, B.; Zimmerman, A.; Harris, W. Biomass-facilitated production of activated magnesium oxide nanoparticles with extraordinary $CO_2$ capture capacity. *Chem. Eng. J.* **2018**, *334*, 81–88. [CrossRef]
27. Xu, X.; Hu, X.; Ding, Z.; Chen, Y.; Gao, B. Waste-art-paper biochar as an effective sorbent for recovery of aqueous Pb(II) into value-added PbO nanoparticles. *Chem. Eng. J.* **2017**, *308*, 863–871. [CrossRef]
28. Wetteland, C.L.; de Jesus Sanchez, J.; Silken, C.A.; Nguyen, N.Y.T.; Mahmood, O.; Liu, H. Dissociation of magnesium oxide and magnesium hydroxide nanoparticles in physiologically relevant fluids. *J. Nanopart. Res.* **2018**, *20*, 215. [CrossRef]
29. Bhatte, K.D.; Sawant, D.N.; Deshmukh, K.M.; Bhanage, B.M. Additive free microwave assisted synthesis of nanocrystalline $Mg(OH)_2$ and MgO. *Particuology* **2012**, *10*, 384–387. [CrossRef]
30. Wang, C.; Wang, H.; Cao, Y. Pb(II) sorption by biochar derived from Cinnamomum camphora and its improvement with ultrasound-assisted alkali activation. *Colloids Surf. A Phys. Eng. Asp.* **2018**, *556*, 177–184. [CrossRef]
31. Bogusz, A.; Oleszczuk, P.; Dobrowolski, R. Application of laboratory prepared and commercially available biochars to adsorption of cadmium, copper and zinc ions from water. *Bioresour. Technol.* **2015**, *196*, 540–549. [CrossRef]
32. Cao, X.; Harris, W. Properties of dairy-manure-derived biochar pertinent to its potential use in remediation. *Bioresour. Technol.* **2010**, *101*, 5222–5228. [CrossRef] [PubMed]
33. Shen, Y.; Zhao, P.; Shao, Q. Porous silica and carbon derived materials from rice husk pyrolysis char. *Microporous Mesoporous Mater.* **2014**, *188*, 46–76. [CrossRef]
34. Tan, Y.; Yin, X.Q.; Wang, C.Y.; Sun, H.M.; Ma, A.S.; Zhang, G.L.; Wang, N. Sorption of cadmium onto Mg-Fe Layered Double Hydroxide (LDH)-Kiwi branch biochar. *Environ. Pollut. Bioavailab.* **2019**, *31*, 189–197. [CrossRef]
35. Harikishore Kumar Reddy, D.; Lee, S.M. Magnetic biochar composite: Facile synthesis, characterization, and application for heavy metal removal. *Colloids Surf. A Phys. Eng. Asp.* **2014**, *454*, 96–103. [CrossRef]
36. Liu, Y.; Zeng, G.M.; Tang, L.; Cai, Y.; Pang, Y.; Zhang, Y.; Yang, G.; Zhou, Y.Y.; He, X.X.; He, Y. Highly effective adsorption of cationic and anionic dyes on magnetic Fe/Ni nanoparticles doped bimodal mesoporous carbon. *J. Colloid Interface Sci.* **2015**, *448*, 451–459. [CrossRef]
37. Zhou, Z.; Liu, Y.G.; Liu, S.B.; Liu, H.Y.; Zeng, G.M.; Tan, X.F.; Yang, C.P.; Ding, Y.; Yan, Z.; Cai, X.X. Sorption performance and mechanisms of arsenic(V) removal by magnetic gelatin-modified biochar. *Chem. Eng. J.* **2017**, *314*, 223–231. [CrossRef]

38. Zhou, Y.; Liu, X.; Wang, P.; Zhang, F.; Wei, J.; Luo, L.; Lei, M.; Tang, L. Modification of biochar derived from sawdust and its application in removal of tetracycline and copper from aqueous solution: Adsorption mechanism and modelling. *Bioresour. Technol.* **2017**, *245*, 266–273. [CrossRef] [PubMed]
39. Zhou, X.; Liu, Y.; Zhou, J.; Guo, J.; Ren, J.; Zhou, F. Efficient removal of lead from aqueous solution by urea-functionalized magnetic biochar: Preparation, characterization and mechanism study. *J. Taiwan Inst. Chem. Eng.* **2018**, *91*, 457–467. [CrossRef]
40. El Saliby, I.; Erdei, L.; Kim, J.H.; Shon, H.K. Adsorption and photocatalytic degradation of methylene blue over hydrogen-titanate nanofibres produced by a peroxide method. *Water Res.* **2013**, *47*, 4115–4125. [CrossRef]
41. Zhang, C.; Wang, W.J.; Duan, A.B.; Zeng, G.M.; Huang, D.L.; Lai, C.; Tan, X.F.; Cheng, M.; Wang, R.Z.; Zhou, C.Y.; et al. Adsorption behavior of engineered carbons and carbon nanomaterials for metal endocrine disruptors: Experiments and theoretical calculation. *Chemosphere* **2019**, *222*, 184–194. [CrossRef]
42. Xiao, Z.; Yang, J.; Ren, R.; Li, J.; Wang, N.; Chu, W. Facile synthesis of homogeneous hollow microsphere Cu–Mn based catalysts for catalytic oxidation of toluene. *Chemosphere* **2020**, *247*, 125812. [CrossRef] [PubMed]
43. Yin, Z.; Liu, Y.G.; Liu, S.B.; Jiang, L.H.; Tan, X.F.; Zeng, G.M.; Li, M.F.; Liu, S.J.; Tian, S.R.; Fang, Y. Activated magnetic biochar by one-step synthesis: Enhanced adsorption and coadsorption for 17β-estradiol and copper. *Sci. Total Environ.* **2018**, *639*, 1530–1542. [CrossRef] [PubMed]